Preparation of Highly Open Porous Styrene/Acrylonitrile and Styrene/Acrylonitrile/Organoclay Polymerized High Internal Phase Emulsion (PolyHIPE) Foams via Emulsion Templating

Z. Abbasian, M. R. Moghbeli

School of Chemical Engineering, Iran University of Science and Technology, P.O. Box 16844-13114, Tehran, Iran

Received 30 September 2009; accepted 21 July 2010
DOI 10.1002/app.33086
Published online 6 October 2010 in Wiley Online Library (wileyonlinelibrary.com).

ABSTRACT: Highly open porous crosslinked styrene/acrylonitrile (SAN) polymerized high internal phase emulsion (PolyHIPE) foams containing various amounts of acrylonitrile (AN) were prepared by the polymerization of the continuous organic phase of high internal phase emulsions with an 85 vol % aqueous internal phase. The mean diameter of voids varied in the range 12.4–19.8 μm. The void diameter increased up to 10% AN, but beyond this limit, the diameter decreased. To improve the mechanical properties of the copolymer foams, the organic phase of the emulsion containing 20% AN was reinforced with organomontmorillonites with different surface modifiers. The effects of the organoclay on the equilibrium torque value of the emulsifying systems, as an approximate characteristic of the emulsion viscosity, and on the morphology and mechanical properties of the resulting foam were investigated. Scanning electron micrographs exhibited an open-cell polyHIPE structure for all of the SAN/organoclay polyHIPE foams. The incorporation of organoclays within the emulsion copolymer foam significantly decreased the mean size of voids and intercellular pores compared with those of the copolymer foam without reinforcement. In fact, the presence of organoclay may have acted as a cosurfactant to improve the performance of the nonionic surfactant in the concentrated emulsions. The X-ray diffraction patterns and transmission electron micrographs showed an intercalated nanocomposite structure for the organoclay-reinforced copolymer foams. On the other hand, the addition of a more hydrophilic organoclay, that is, 3 wt % Cloisite30B, to the concentrated emulsion decreased the Young's modulus and significantly improved the crush strength of the emulsion copolymer foam. © 2010 Wiley Periodicals, Inc. J Appl Polym Sci 119: 3728–3738, 2011

Key words: copolymerization; emulsion polymerization; nanocomposites

INTRODUCTION

High internal phase emulsions (HIPEs) are emulsions with an internal phase volume ratio greater than 74% of the total emulsion volume. Through the polymerization of the continuous phase of HIPEs and then the removal of the internal phase, polymers of high internal phase emulsions (polyHIPEs) with a cellular structure are produced.[1,2] PolyHIPEs are useful for many applications, such as insulation, tissue engineering supports, separation process, ion-exchange modules, and separation media, because of their highly interconnected porous structure and easy production.[3–8] The effect of crucial parameters, such as the nature and concentrations of the surfactant, crosslinking agent, electrolyte, and porogenic solvents and emulsion preparation conditions, on the morphology and properties of polyHIPE foams have been investigated.[9–15] Most of these studies were based on styrene (St)/divinylbenzene (DVB) polyHIPE foams and a few copolymer foams containing a more hydrophilic comonomer, such as alkylmaleimides and 2-ethylhexyl acrylate.[16–19]

Few studies have been conducted to improve the thermomechanical properties of highly porous polyHIPE foams. Tai et al.[20] synthesized an open-cell hybrid foam composed of an inorganic polysilsesquioxane network in combination with an organic polystyrene (PS) network via emulsion templating. This modification method considerably increased the high-temperature modulus and improved the thermal stability of the resulting hybrid foams. Lepine et al.[21] prepared an elastomeric interpenetrating network polyHIPE solid foam by adding a PS network to the polyurethane (PU) network to modify the dimensional stability of the resulting PU–PS foam. In this case, the use of hydroxybutyl methacrylate as a comonomer that chemically linked both networks resulted in the formation of an interpenetrating network polyHIPE solid foam. The Young's modulus of the PU–PS polyHIPE

Correspondence to: M. R. Moghbeli (mr_moghbeli@iust.ac.ir).

TABLE I
Recipes for the Preparation of the PolyHIPE Foams

	Oil phase (g)				Aqueous phase (g)			Clay (wt %)	
Code	St	DVB	AN	Span80	DDI	$CaCl_2$	$K_2S_2O_8$	C15A	C30B
1	3.171	0.317	0.0	0.7	69.425	0.435	0.14	—	—
2	3.012	0.317	0.158	0.7	69.425	0.435	0.14	—	—
3	2.854	0.317	0.317	0.7	69.425	0.435	0.14	—	—
4	2.537	0.317	0.634	0.7	69.425	0.435	0.14	—	—
5	2.537	0.317	0.634	0.7	69.425	0.435	0.14	1	0
6	2.537	0.317	0.634	0.7	69.425	0.435	0.14	2	0
7	2.537	0.317	0.634	0.7	69.425	0.435	0.14	3	0
8	2.537	0.317	0.634	0.7	69.425	0.435	0.14	0	1
9	2.537	0.317	0.634	0.7	69.425	0.435	0.14	0	2
10	2.537	0.317	0.634	0.7	69.425	0.435	0.14	0	3

was three times higher than that of the conventional PS polyHIPE foam with the same internal-phase volume fraction. Wang et al.[22] prepared a highly porous monolithic carbonaceous scaffold by carbonization of poly(styrene–divinylbenzene) polyHIPEs. Silverstein et al.[23] synthesized polyHIPE silica foams to enhance their mechanical properties and extend the temperature range of damping of the resulting foams. Moreover, they improved the high-temperature mechanical properties of the foams through the synthesis of a hybrid polyHIPE containing an inorganic silsesquioxane network. Menner et al.[24] synthesized reinforced polyHIPEs by varying the amount of methacryloxypropyltrimethoxysilane, St, and DVB within the concentrated emulsions. Recently, Haibach et al.[25] used nanosilica particles along with a silane coupling agent to reinforce the organic phase of polyHIPE foams. The nanosilica particles considerably increased the Young's modulus and crush strength (σ_{cr}) of the foam in comparison with the foam without reinforcement. In another study, Menner et al.[26] synthesized porous nanocomposite foams using carbon nanotubes (CNTs). CNTs, as intrinsically hydrophobic nanofibers, are convenient for stabilizing water/oil concentrated emulsions. The addition of CNTs not only eliminated the need for traditional nonionic surfactants but also increased the mechanical and electrical properties of the polyHIPE foams. Recently, typical layered silicate particles, such as natural and organically modified montmorillonites, have been introduced at different concentrations to control the microstructure of rigid poly(styrene–divinylbenzene) polyHIPE solid foams.[27] It is believed that the open-cell contents increased as the organoclay level increased because of the decreasing viscosity ratio of the dispersed to continuous phases in the HIPEs.

Although many scientists have investigated the effects of the emulsion composition on the polyHIPE microstructure and properties, less or no attention has been paid to the effect of layered silicate nanoclays on the microstructure and properties of styrene/acrylonitrile (SAN) polyHIPE foams. In this study, we investigated the effects of a more hydrophilic comonomer, that is, acrylonitrile (AN), and organically modified nanoclays on the HIPE viscosity and polyHIPE morphology and properties.

EXPERIMENTAL

Materials

All reagents were purchased from Merck Co. (Darmstadt, Germany), unless otherwise stated. St, DVB, and AN were distilled *in vacuo* before use. Sorbitan monoleate (Span80) as a nonionic surfactant, potassium persulfate ($K_2S_2O_8$) as a water-soluble initiator, and an electrolyte ($CaCl_2.4H_2O$) were used without any additional purification. Organically modified sodium montmorillonite (NaMMT), Cloisite15A (C15A), and Cloisite30B (C30B) organoclays were used to reinforce the organic phase of the foams. In all recipes, distilled deionized water (DDI) was used.

HIPE preparation

Table I shows the recipes for the preparation of the SAN and SAN/organoclay polyHIPE solid foams. The continuous organic phase of HIPE consisted of AN, St, DVB, and the emulsifier, and the dispersed aqueous phase consisted of the initiator, DDI, and the electrolyte. As shown, the AN content in the emulsions varied in the range 0–20 wt % on the basis of the total monomer content. The weight ratio of the monomer to the crosslinker in all emulsion samples was held at 10 : 1, and the continuous phase was 10% of the total emulsion volume. To prepare the foam emulsion, the aqueous phase was added dropwise to the organic phase with a continuous stirring speed of 1000 rpm. Once all the internal phase was added, stirring was continued for 5 min more to obtain a homogeneous emulsion. For the preparation of the polyHIPE nanocomposite foams,

various organoclay levels (1–3 wt % on the basis of the total monomer content) were added to the organic phase. For this purpose, the organoclay was dispersed in the monomer with a magnetic stirrer at 400 rpm for 12 h, and then, Span 80 was added to the dispersion and stirred vigorously by a mechanical stirrer at 2000 rpm for 24 h.

PolyHIPE preparation

All prepared HIPEs were poured into the prepared glass molds. The sealing of the molds was necessary for the polymerization reaction. The emulsions were cured at 75°C in a circulating oven for 24 h and then, dried in a vacuum oven at 85°C for 48 h.

The overall polymerization conversion (X) was determined on the basis of the gravimetrical measurements with the following equation:

$$X = \frac{w_d(w_a - w_c)}{w_m w_b} \times 100 \quad (1)$$

where w_m is the mass of the monomers in the concentrated emulsion, w_d is the mass of the dried solid foam, w_b is the mass of the sample before Soxhlet extraction, w_a is the mass of the sample after extraction, and w_c is the mass of the organoclay inside the sample prepared after extraction. The Soxhlet extraction was carried out for 24 h in DDI followed by 24 h in methanol to remove the residual monomers and the emulsifier.[23]

Characterization

PolyHIPE microstructure

The morphology of the polyHIPE solid foams was studied by means of scanning electron microscopy (Philips XL30 SEM, Eindhoven, Netherlands). For this purpose, the solid foam was frozen in liquid nitrogen and fractured. The fractured surface was then gold-sputtered before microscopy. The mean sizes of the voids were measured from the SEM images of 300 voids for each foam sample according to the following equations.[28]

$$\overline{D_n} = \left(\sum_i N_i D_i\right) / \left(\sum_i N_i\right) \quad (2)$$

$$\overline{D_w} = \left[\left(\sum_i N_i D_i^6\right) / \left(\sum_i N_i D_i^3\right)\right]^{1/3} \quad (3)$$

$$\mathrm{PDI} = \overline{D_w}/\overline{D_n} \quad (4)$$

where $\overline{D_n}$ and $\overline{D_w}$ are the number- and weight-average void sizes, respectively; N_i is the number of voids with D_i diameter; and the polydispersity index (PDI) is a criterion of the void size distribution within the polyHIPE foam.

The organoclay dispersion in the foam copolymer matrix was investigated by means of transmission electron microscopy (TEM). For this purpose, ultrathin sections of the solid foam filled with an epoxy resin were prepared and transferred onto a 400-mesh copper grid and dried in open air for 2 h before microscopy observation.

A Zeiss TEM CEM 902A (Oberkochen, Germany) with an acceleration voltage of 120 kV was used.

PolyHIPE properties

We measured the apparent density of the foams by measuring the weight and volume of the samples. The thermal conductivity of the foam samples was measured with a thermal conductivity apparatus. The technique used to measure the thermal conductivity was based on the rate of steady-state heat transfer across a known thickness, induced by two different known temperatures at two opposite surfaces of the foam. The test specimens were in the form of plates with a thickness of 3 mm. Compression tests were carried out according to standard ASTM D 1621-94 on an MTS testing machine (MTS 810, Minneapolis, MN) equipped with a 10-kN load cell. The compressive stress–strain measurements were performed on cylindrical foam specimens 60 mm in diameter and 30 mm in height at room temperature. At least three specimens were used for each foam. The initial linear slope of the compression stress–strain curves and the stress at yield point were reported as the Young's modulus and σ_{cr} of the foams, respectively. The thermal stability of the polyHIPE foams was studied with a PerkinElmer thermal analyzer (Waltham, MA) at a heating rate of 10°C/min under a nitrogen atmosphere. X-ray diffraction (XRD; Siemens D5000, Munich, Germany) experiments were carried out to investigate the nanostructure of the resulting nanocomposite foams. In this case, the reinforced polyHIPE sample was placed at −16°C for 24 h and was then ground into very fine powder. The powder samples were dried *in vacuo* to remove traces of moisture before the experiment. The crystallographic spacing (d-spacing) between the silicate layers of the organoclays was determined on the basis of Bragg's law:

$$\lambda = 2d \sin\theta$$

where λ is the wavelength of incident wave, and θ is the angle between the incident ray and the scattering planes.

RESULTS AND DISCUSSION

The continuous organic phase of emulsions 1–4 contained various amounts of AN comonomer (0, 5, 10, and 20 wt %) and St, DVB, and Span80 as a nonionic surfactant (Table I). The conversions of the all of the foam emulsions determined by gravimetric

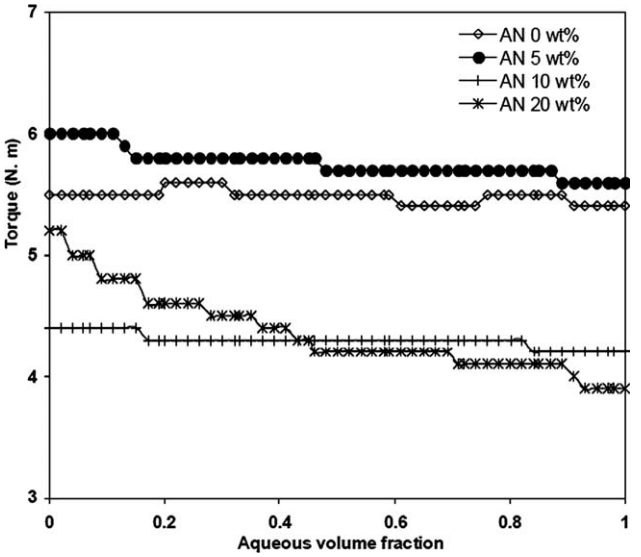

Figure 1 HIPE torque variations versus the aqueous-phase volume fraction for the concentrated emulsions prepared with various levels of AN.

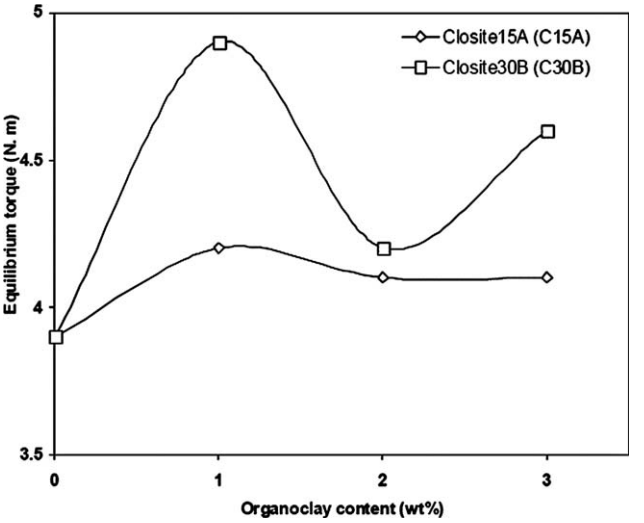

Figure 3 Effect of the organoclay level on the torque of the concentrated emulsions.

measurement were in the range 97–99%. A progressive free-radical emulsion copolymerization within the concentrated water/oil emulsion template produced a polymer network with sufficient structural integrity to prevent the collapse of the forming solid foam. The phase separation in the polymerizing organic phase supported a large number of spherical intercellular pores in the resulting emulsion solid foam.

To improve the properties of the SAN (20 wt % AN) copolymer foam, hybrid C15A and C30B organoclays with different surface hydrophilicities were used as inorganic fillers. The volume fraction of the aqueous internal phase in all of the recipes was kept constant at 85 vol %. An additional electrolyte, $CaCl_2 \cdot 4H_2O$, was used to suppress Ostwald ripening and enhance the stability of the concentrated emulsions. All of the organoclay-reinforced emulsion templates and the emulsion without reinforcement were cured at the same polymerization temperature of 75°C for 24 h.

HIPE torque variations

The rheological behavior of the emulsions during the emulsification process with the continuous addition of an aqueous droplet phase was evaluated approximately by the torque values, which were measured automatically. The value of equilibrium torque as an

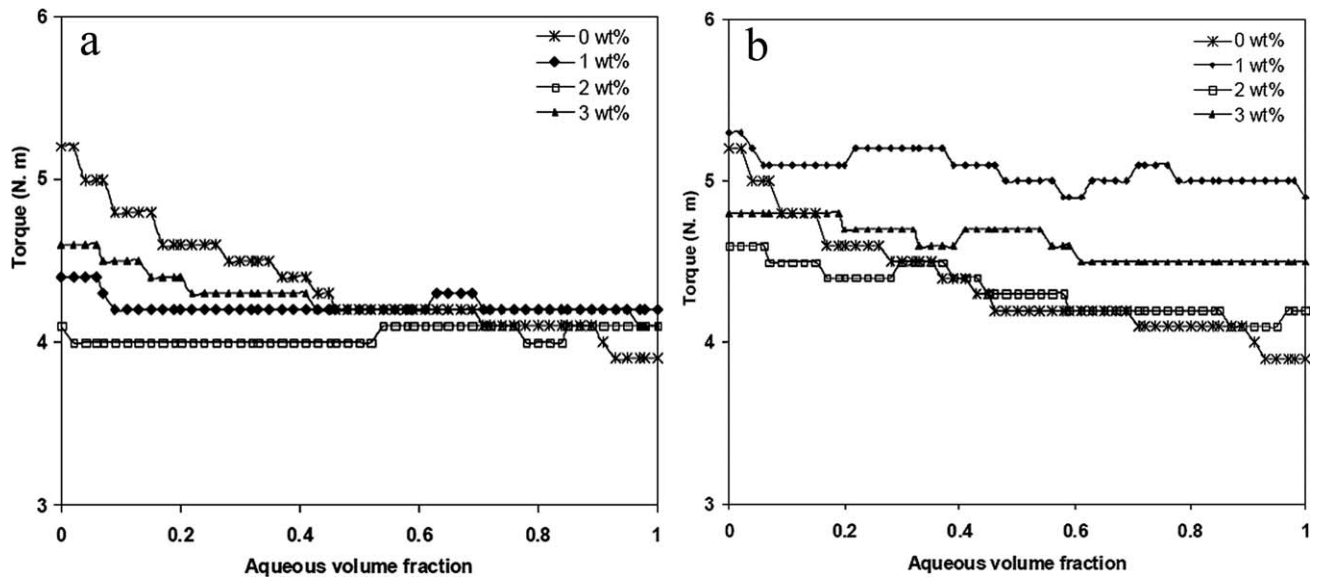

Figure 2 HIPE torque variations versus the aqueous-phase volume fraction for the concentrated SAN20 and various levels of organoclays: (a) C15A and (b) C30B.

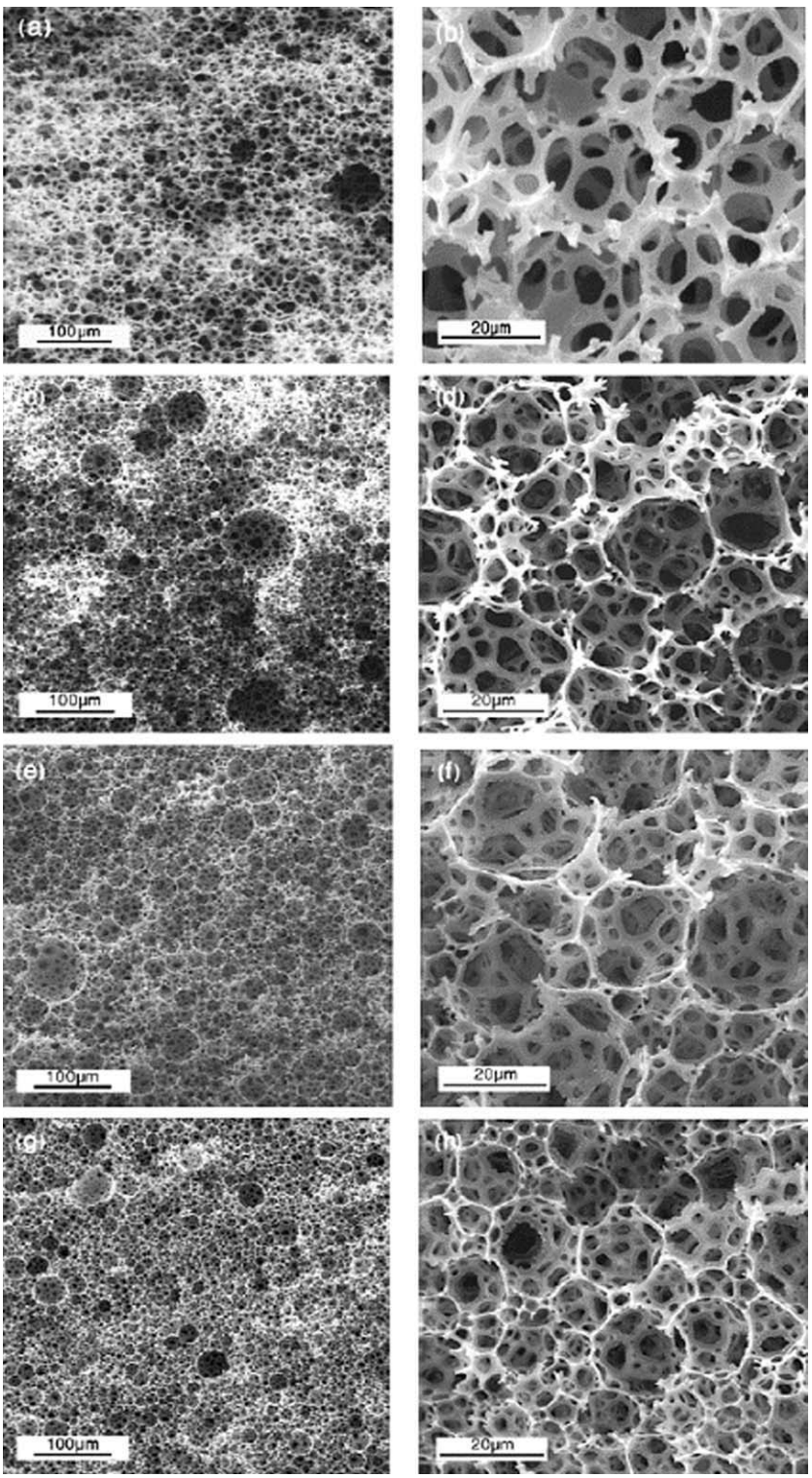

Figure 4 SEM micrographs of the polyHIPE foams containing various amounts of AN comonomer: (a,b) 0, (c,d) 5, (e,f) 10, and (g,h) 20 wt %.

approximate characteristic value of the emulsion viscosity can represent the stability of the concentrated emulsions. Figure 1 shows the torque variations of emulsions prepared with various amounts of AN versus the aqueous volume fraction during the emulsification process at 25°C. As shown, the highest torque values were observed for the emulsion containing 5 wt % AN compared with other foam emulsions with lower or higher AN contents. This observation implied that the extent of AN solubility in the aqueous dispersed phase, here close to 5%, was a key parameter in determining the viscosity of the

TABLE II
Characteristics of the Prepared PolyHIPE Foams

Code	$\overline{D_n}$ (μm)	PDI	$\overline{d_n}$ (μm)	$\overline{d_n}/\overline{D_n}$	$\sigma_{cr} \times 10^2$ (g/cm^3)	$\kappa \times 10^2$ (W m^{-1} k^{-1})	E (MPa)	$\sigma_{cr} \times 10^2$ (MPa)
1	13.4 ± 0.6	1.35	2.9 ± 0.1	0.21	6.1 ± 0.2	66 ± 6	3.2 ± 0.3	9 ± 0.3
2	13.2 ± 0.4	1.77	2.9 ± 0.3	0.22	6.5 ± 0.2	55 ± 3	5.7 ± 0.1	4 ± 0.1
3	19.8 ± 0.6	1.82	2.9 ± 0.1	0.15	6.8 ± 0.4	57 ± 2	2.9 ± 0.2	23 ± 0.4
4	12.4 ± 0.3	2.22	2.1 ± 0.1	0.17	8.7 ± 0.5	63 ± 5	4.3 ± 0.1	8 ± 0.2
5	8.6 ± 0.2	1.79	2.0 ± 0.2	0.23	6.6 ± 0.4	51 ± 3	3.3 ± 0.2	5 ± 0.2
6	6.9 ± 0.2	2.43	1.7 ± 0.1	0.24	7.5 ± 0.3	50 ± 6	4.7 ± 0.1	18 ± 0.5
7	7.8 ± 0.1	2.61	1.9 ± 0.1	0.25	7.4 ± 0.5	50 ± 5	2.3 ± 0.2	9 ± 0.3
8	8.2 ± 0.3	2.11	1.7 ± 0.2	0.21	6.8 ± 0.4	51 ± 3	2.2 ± 0.1	18 ± 0.2
9	7.6 ± 0.2	1.83	1.5 ± 0.1	0.20	8.5 ± 0.6	53 ± 4	3.7 ± 0.1	13 ± 0.3
10	8.0 ± 0.1	1.60	2.0 ± 0.1	0.24	5.6 ± 0.4	50 ± 3	3.0 ± 0.2	19 ± 0.4

ρ = foam density; κ = foam thermal conductivity; E = Young's modulus.

concentrated emulsions. Increasing the AN content above 5 wt % in the organic phase of the emulsions caused the torque value to decrease. This behavior was attributed to the decrease in the interfacial tension between the two phases due to the AN level increase. The highest decrease in the equilibrium torque was observed for the SAN emulsion prepared with the highest AN level, 20 wt % (Fig. 1).

The incorporation of organoclay into the SAN emulsion containing 20% AN (SAN20) had a considerable effect on the rheological behavior of the emulsifying systems, which was dependent on the type and amount of the organoclay used. Figure 2 indicates the effect of additional organoclay on the viscosity variation of the concentrated emulsions versus the aqueous volume fraction. Interestingly, small changes in the torque values were observed for the emulsions containing organoclays during the emulsifying process compared with emulsion 4, without organoclay. One can imagine that using the organoclay could decrease the emulsion instability originating from the presence of a higher level of AN comonomer in the continuous phase. In addition, the preferred absorption of AN compared with hydrophobic St within the preswelled silicate layers of the organoclays, especially for the more hydrophilic C30B, was another reason that the stability of the reinforced emulsions was enhanced. An increase in the percentage of the organoclay enhanced the torque value to some extent once all of the aqueous phase was added (Fig. 3). Nevertheless, in the early stages of the emulsifying process with lower water/oil phase ratios, the torque of the emulsions with higher levels of nanoclay was significantly lower than that of the emulsion without reinforcement (Fig. 2). A further increase in the emulsion viscosity was observed for the emulsions containing C30B with hydroxyl functionality compared with the emulsions containing C15A without functional groups. In fact, the use of more a hydrophilic organoclay increased the organic/inorganic thermodynamic interactions in the continuous phase and caused the emulsion viscosity to increase.

Morphology of the SAN polyHIPE foams

Figure 4 shows the SEM micrographs of polyHIPE foams prepared with various amounts of AN levels in the continuous organic phase. The emulsion foam 1 without AN comonomer [Fig. 4(a,b)] was synthesized as a reference sample to evaluate the effect of the comonomer on the foam microstructure and properties. As shown, open-cell structures of polyHIPE were observed for all of the SAN polyHIPE foams and the polyHIPE foam 1. In addition, the wall thickness of the voids seemed to decrease considerably with increasing AN content. In fact, the presence of a more hydrophilic commoner led to the thinning of the continuous organic film separating individual internal phase droplets because of the decrease of water/oil interfacial tension within the concentrated emulsions. A quantitative description of the cell structure of the low-density copolymer foams is summarized in Table II. As shown, the mean diameter of voids varied from 12.4 to 19.8 μm. The void diameter ($\overline{D_n}$) increased up to 10% AN, but beyond this limit, the void diameter decreased. The void size distribution was broadened as the AN% increased due to Ostwald ripening, whereas no significant change in the size of the intercellular pores ($\overline{d_n}$) was observed. In addition, the degree of foam network interconnection, as expressed by the $\overline{d_n}/\overline{D_n}$ ratio, decreased for the copolymer foams with higher AN contents (Table II and Fig. 4).

Morphology of the nanocomposite foams

As mentioned earlier, the incorporation of the organoclays within the continuous organic phase enhanced the emulsion viscosity as the organoclay level increased. It is possible that the monomers to be polymerized into the montmorillonite galleries of the preswelled organoclay in addition to the polymerization progressed in the organic media out of the organoclay. In fact, the polymerization in such a heterogeneous continuous phase seems to be very

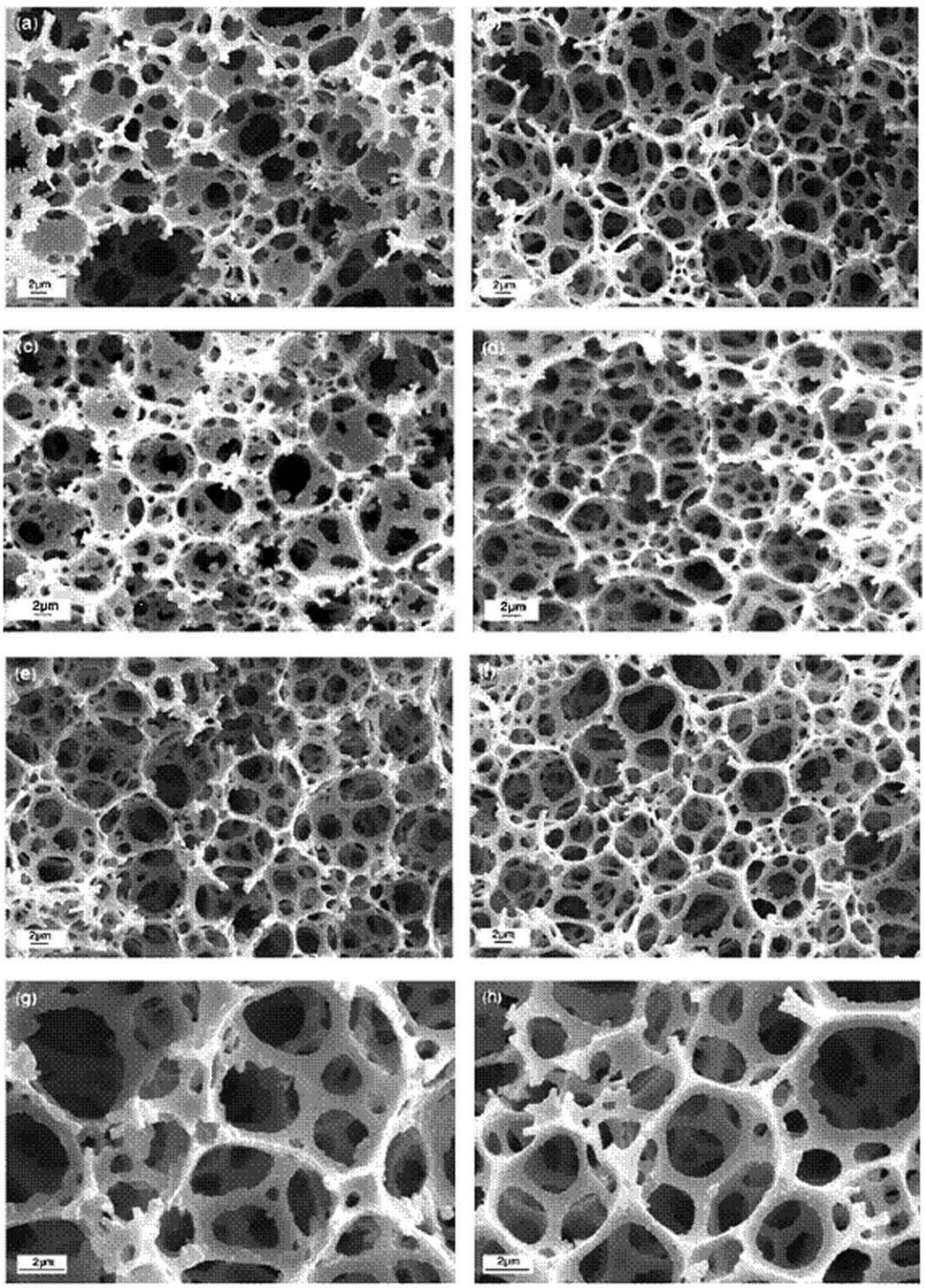

Figure 5 SEM micrographs of the SAN20/organoclay polyHIPE nanocomposite foams containing various levels of organoclay: (a) 1 wt % C15A, (b) 1 wt % C30B, (c) 2 wt % C15A, (d) 2 wt % C30B, (e,g) 3 wt % C15A, and (f,h) 1 wt % C30B.

complex because of the probable differences in the chemical compositions of the reactants and the polymerization rate in both of the reacting regions.[29,30] Because of the significant decrease in the polymerization rate of the reinforced emulsion templates to achieve sufficient mechanical properties, the polymerization temperature and time were increased for all emulsion samples (Table I). Figure 5 shows that emulsion foams 5–10, prepared with various levels of organoclay, had an open-pore cell structure with a high degree of network interconnectivity. The addition of various levels of organoclays to SAN20

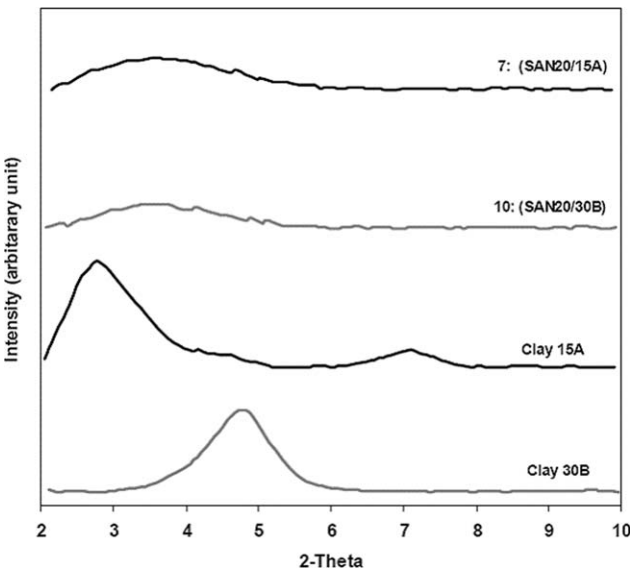

Figure 6 XRD patterns of SAN20/Org-MMT polyHIPE nanocomposite foams (15A = Cloisite15A; 30B = Cloisite30B).

significantly decreased the mean void diameter compared to the emulsion without reinforcement (Table II). For the polyHIPE foams containing up to 2% C15A, the mean void diameter decreased to 6.9 μm, but further increases in the organoclay content led to an increase in the void diameter to 8.1 μm. The same variation in the size of intercellular pores in the range 1.1–2 μm was observed with increasing organoclay content. On the other hand, PDI of the void diameter increased with increasing organoclay content, as shown in Figure 5. In contrast, an increase in the C30B level decreased the broadness of the void size distribution and enhanced the degree of network interconnectivity. Interestingly, although the addition of C30B to emulsion 4 enhanced the emulsion viscosity (Fig. 3), it significantly decreased the void diameter in the reinforced foams (Table II). The mean size of the intercellular pores and the network interconnectivity increased for the reinforced foams with increasing content of the more hydrophilic organoclay (Table II). These observations implied that the C30B nanoparticles may have acted as a cosurfactant to improve the performance of the nonionic surfactant in the emulsions containing AN comonomer. In this case, the organoclay particles may have been orientated toward the water/oil interface. This was also clearly visible from the inspection of the SEM micrographs, in which the addition of C15A to the formulation of the emulsions, in comparison with the addition of C30B, considerably decreased the density of the intercellular pores in the porous foams [Fig. 5(a–d)]. The presence of the organoclay seemed to increase the strength of the void wall and, hence, decrease the number of intercellular pores formed during the drying process of the polymerized emulsion templates. Nevertheless, the incorporation of the more hydrophilic organoclay led to the formation of solid foams with thinner intercellular walls and a higher network interconnectivity. As shown at a larger magnification, the foam containing C30B had a different internal surface structure than the foam reinforced with C15A [Fig. 5(g,h)]. A higher smooth internal surface of voids and a uniform intercellular pore edge were clearly observed for the foams reinforced by the more hydrophilic organoclay. Nevertheless, both organoclay particles seemed to be integrated into the pore walls of the reinforced emulsion foams.

XRD patterns of the crosslinked SAN polyHIPE foams reinforced with 3 wt % organomontmorillonite (Org-MMT) revealed an intercalated layered silicate nanocomposite (Fig. 6). As shown, an increased interlayer spacing of Org-MMTs after polymerization of the HIPE/Org-MMT mixtures was observed because of the formation of SAN copolymer chains into the montmorillonite galleries. In this case, (001) diffraction peaks (2θ's) existed at 7.10 and 4.86° and were related to *d*-spacings of 12.44 and 18.16 Å for the

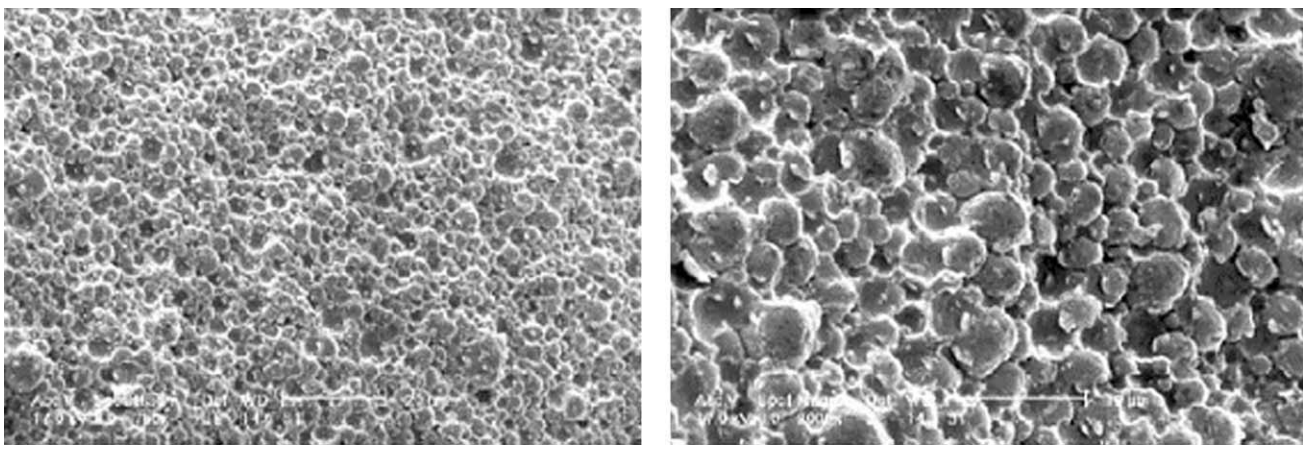

Figure 7 SEM micrographs of the SAN20/C30B (3%) polyHIPE foam filled with an epoxy resin.

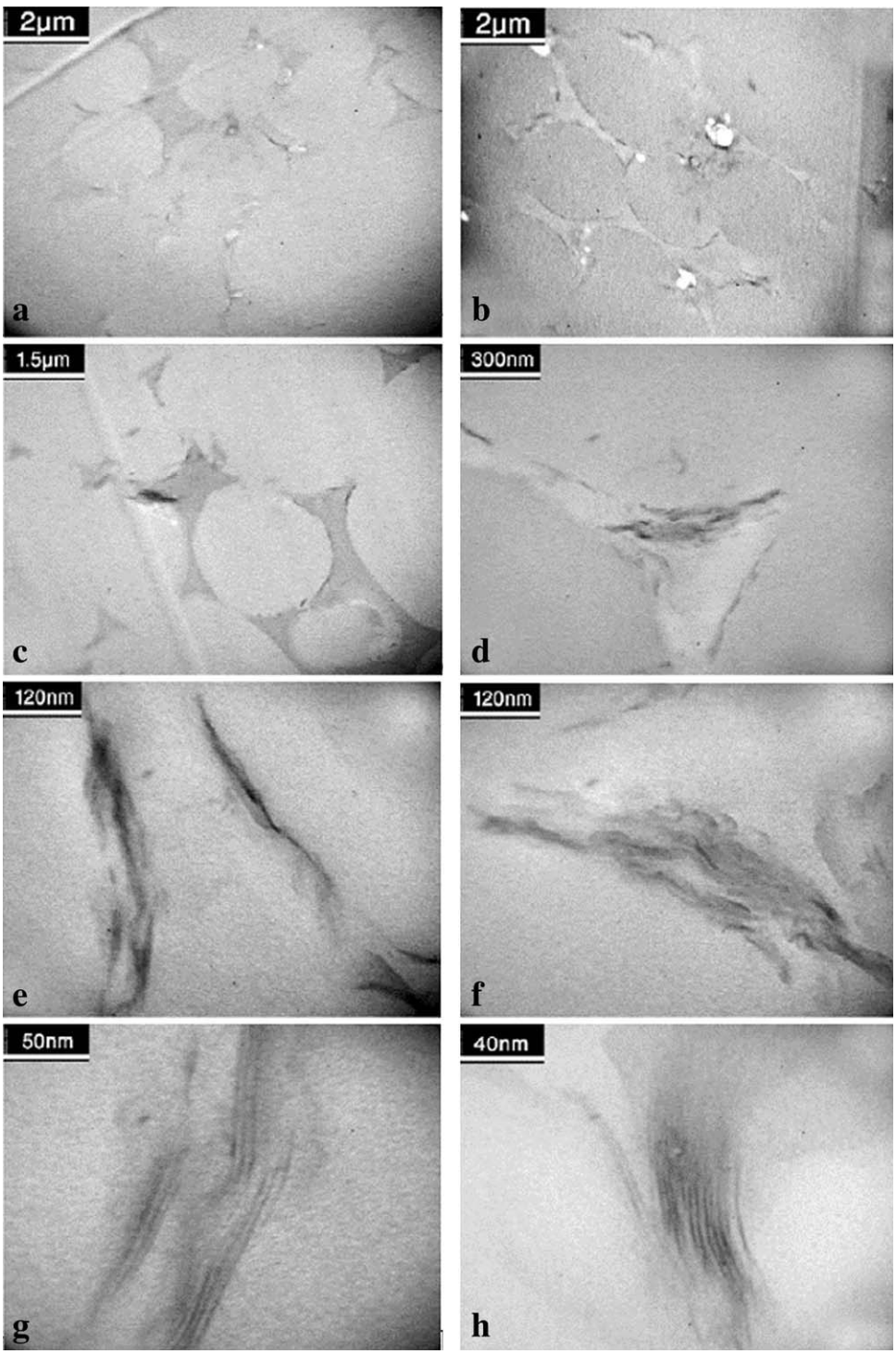

Figure 8 TEM micrographs of the SAN20/C30B polyHIPE foams filled with an epoxy resin: (a) 1 and (b) 3 wt % C30B.

C15A and C30B organoclays, respectively. For the nanocomposite foam containing the former organoclay, a lower 2θ (3.68°) and a higher *d*-spacing (d = 23.97 Å) were obtained than with the surface-treated NaMMT (Fig. 6). Nevertheless, a higher tendency between the SAN copolymer chains and the more hydrophilic organoclay in the solid nanocomposite foams led to a higher *d*-spacing (d = 25.73 Å).

TEM micrographs revealed more information about the organoclay dispersion and delamination within the void walls. For this purpose, the open-cell foam was filled with an epoxy resin to provide suitable ultrathin sections for microscopy observation (Fig. 7). The TEM micrographs showed the cellular morphology, in which the spherical voids merged together to a great extent to form an interconnected network

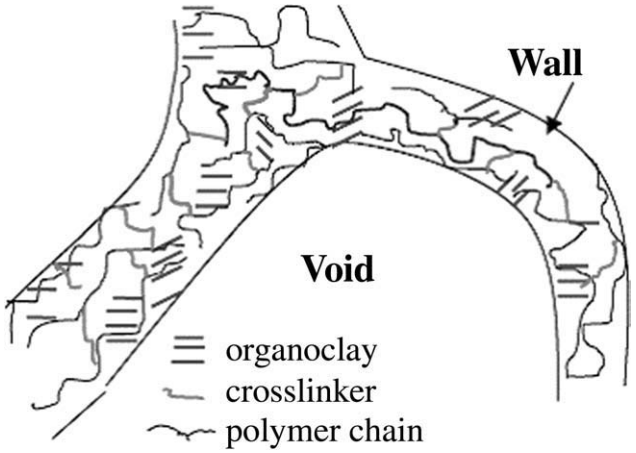

Figure 9 Schematic representation of the SAN polyHIPE nanocomposite foam.

structure [Figs. 8(a,b)]. As shown, the organoclay material, as the dark stacks of silicate layers, was restricted in the void walls [Figs. 8(c,d)]. At higher magnification, the agglomeration of the organoclay stacks was observed inside the copolymer matrix, especially for the higher organoclay level, that is, 5 wt % [Fig. 8(f)]. The magnified TEM images exhibited an intercalated nanocomposite structure for the resulting organoclay-reinforced copolymer foams [Figs. 8(g,h)]. One can imagine that obtaining the exfoliated layered nanocomposite foam could lead to much more superior thermal and mechanical properties compared with those of the intercalated layer nanocomposite structure obtained (Fig. 9).

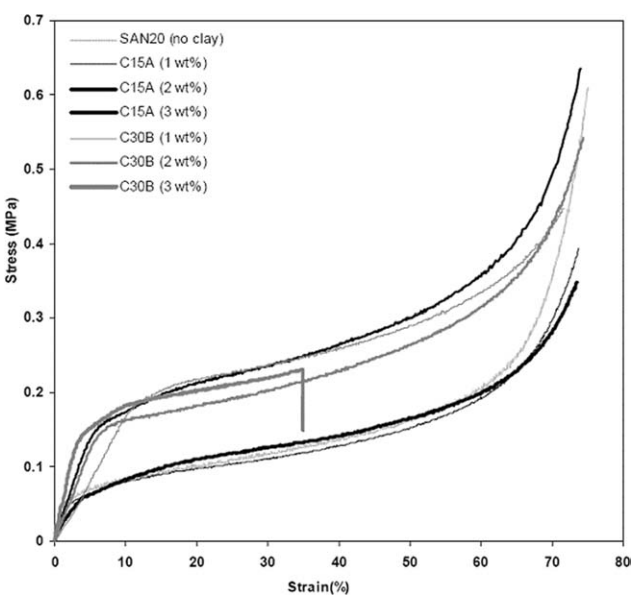

Figure 10 Compressive stress–strain curves of the SAN20 polyHIPE nanocomposite foams reinforced with various levels of C15A and C30B.

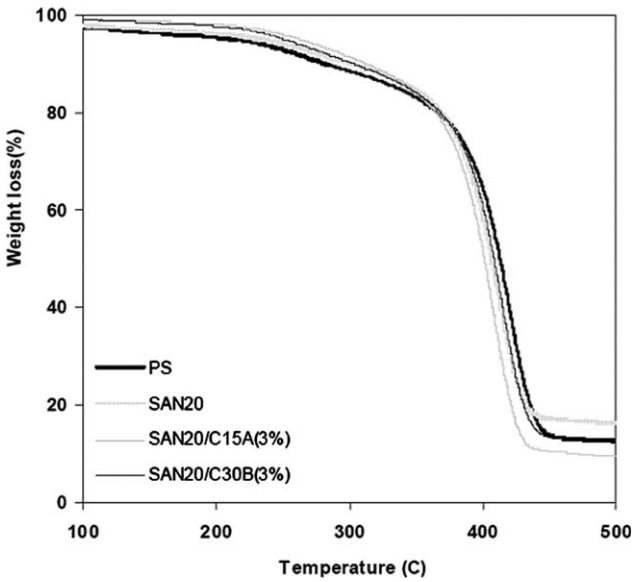

Figure 11 TGA thermograms of the polyHIPE foams with and without reinforcement.

PolyHIPE properties

The physical properties of the crosslinked SAN polyHIPE foams with various levels of AN comonomer and organoclays are shown in Table II. An increase in the apparent foam density from 0.061 to 0.087 g/cm^3 was observed for the copolymer foams as the AN level increased. The foam thermal conductivity decreased up to 5% AN, but beyond this limit, the thermal conductivity increased. The incorporation of AN in emulsion recipes 2–4, except for recipe 3 containing 10% AN, reduced σ_{cr} of the corresponding solid foams compared with foam 1 without AN comonomer (Table II). The increase in the heterogeneity in the cell structure of the copolymer foams due to an increase in the polydispersity in the size of voids and the decrease in the void wall thickness, both arising from the presence of AN, caused the foam σ_{cr} to decrease. Larger voids surrounded by smaller ones in porous foams act as weak points to build up stress concentration under low applied compressive loads.

The incorporation of the organoclay within the polyHIPE porous materials decreased the foam apparent density and thermal conductivity (Table II). The addition of various levels of C15A to SAN20 had an inverse effect on the mechanical properties of the resulting nanocomposite foams, except for the copolymer foam reinforced with 2 wt % organoclay (Fig. 10). Surprisingly, the incorporation of a higher level of C30B considerably increased the compressive properties of the nanocomposite foams. The results showed that the addition of the hydrophilic organoclay (3 wt % C30B) to the emulsion considerably enhanced σ_{cr} of the foam compared with the corresponding copolymer foam without reinforcement (Fig. 10 and Table II). The results also show that the addition of

1 and 3 wt % C30B to the copolymer emulsion, in comparison to the same levels of C15A, decreased the Young's modulus but significantly improved σ_{cr}. This behavior may have been due to the higher level of interaction between C30B and the copolymer chains compared to that of C15A.

Thermal stability of polyHIPE

Figure 11 indicates the effects of the AN comonomer and organoclay on the thermal stability of the solid foams. Three weight loss stages were observed for all of the foam samples. The first small weight loss due to moisture removal was in the temperature region 80–150°C. Thermal decomposition of the nonionic surfactant seemed to occur in the intermediate temperature range and varied from 150 to 360°C with the highest weight loss being 18%; this was close to the amount of surfactant used in the emulsion recipes (Table I). In this stage, the lowest and highest thermal stabilities corresponded to emulsion foam 1 without AN comonomer and emulsion nanocomposite foam 7 containing 3 wt % C15A, respectively (Fig. 11). On the contrary, the highest weight loss was observed for the previous nanocomposite foam at temperatures above 360°C compared with solid foam 1 with the lowest amount. This behavior was attributed to the degradation of the organic modifier used in the surface treatment of the organoclay. The products formed during the thermal degradation of the organic modifier accelerated the kinetics of polymer decomposition and reduced the thermal stability of the foams reinforced with the organoclays.

CONCLUSIONS

More hydrophilic, highly open porous polyHIPE foams were prepared by the addition of various levels of AN comonomer to the continuous phase of St/DVB HIPEs. Nevertheless, the presence of AN units in the polyHIPE copolymer foams decreased the mechanical properties compared with the solid foam without AN comonomer, except for the emulsion foam prepared with 10% AN. The reinforcement of concentrated emulsions with organically modified NaMMT had a considerable effect on the morphology and properties of the resulting foams. The incorporation of 3 wt % C30B with SAN20 significantly decreased the mean void diameter and increased the foam network interconnectivity. These observations implied that the clay particles may have acted as cosurfactants to improve the performance of the nonionic surfactant used to stabilize the concentrated emulsions containing AN comonomer. Surprisingly, a significant increase in σ_{cr} was obtained for the previous polyHIPE nanocomposite foam prepared with 3 wt % C30B compared with the copolymer foam without reinforcement. Nevertheless, the addition of organoclay mainly decreased Young's modulus of the nanocomposite foams compared with the corresponding copolymer foam without reinforcement.

References

1. Cameron, N. R. Polymer 2005, 46, 1439.
2. Cameron, N. R.; Sherrington, D. C. Adv Polym Sci 1996, 126, 165.
3. Dyer, J. C.; Desmarais, T. A. U.S. Pat. 5,633, 291 (1997).
4. Akay, G.; Birch, M. A.; Bokhari, M. A. Biomaterials 2004, 25, 3991.
5. Busby, W.; Cameron, N. R.; Jahoda, C. Biomacromolecules 2001, 2, 154.
6. Pulko, I.; Kolar, M.; Krajnc, P. Sci Total Environ 2007, 386, 114.
7. Krajnc, P.; Leber, N.; Stefanec, D.; Kontrec, S.; Podgornik, A. J Chromatogr A 2005, 1065, 69.
8. Wakeman, R. J.; Bhumgara, Z. G.; Akay, G. Chem Eng J 1998, 70, 133.
9. Williams, J. M. Langmuir 1991, 7, 1370.
10. Williams, J. M.; Wrobleski, D. A. Langmuir 1988, 4, 656.
11. Williams, J. M.; Gray, A. J.; Wilkerson, M. H. Langmuir 1990, 6, 437.
12. Barbetta, A.; Cameron, N. R. Macromolecules 2004, 37, 3188.
13. Barbetta, A.; Cameron, N. R. Macromolecules 2004, 37, 3202.
14. Cameron, N. R.; Barbetta, A. J Mater Chem 2000, 10, 2466.
15. Abbasian, Z.; Moghbeli, M. R. J Appl Polym Sci 2010, 116, 986.
16. Barby, D.; Haq, Z. U.S. Pat. 4,522,953 (1985).
17. Duke, J. R.; Hoisington, M. A.; Langlois, D. A.; Benicewicz, B. C. Polymer 1998, 39, 4369.
18. Tai, H.; Sergienko, A.; Silverstein, M. S. Polym Eng Sci 2001, 41, 1540.
19. Cameron, N. R.; Sherrington, D. C. J Mater Chem 1997, 7, 2209.
20. Tai, H.; Sergienko, A.; Silverstein, M. S. Polymer 2001, 42, 4473.
21. Lepine, O.; Birot, M.; Deleuze, H. Polymer 2005, 46, 9653.
22. Wang, D.; Smith, N. L.; Budd, P. M. Polym Int 2005, 54, 297.
23. Silverstein, M. S.; Tai, H.; Sergienko, A.; Lumelsky, Y.; Pavlovsky, S. Polymer 2005, 46, 6682.
24. Menner, A.; Haibach, K.; Powell, R.; Bismarck, A. Polymer 2006, 47, 7628.
25. Haibach, K.; Menner, A.; Powell, R.; Bismarck, A. Polymer 2006, 47, 4513.
26. Menner, A.; Verdejo, R.; Shaffer, M.; Bismarck, A. Langmuir 2007, 23, 2398.
27. Ahmed, M. S.; Lee, Y. H.; Park, C. B.; Atalla, N. Asia-Pac J Chem Eng 2008, 4, 120.
28. Juang, M. S.; Krieger, I. M. J Polym Sci Polym Chem Ed 1976, 14, 2089.
29. Liu, G.; Zhang, L.; Wang, B.; Zhang, Y. J Appl Polym Sci 2003, 90, 3690.
30. Liu, G.; Zhang, L.; Zhao, D.; Qu, X. J Appl Polym Sci 2005, 96, 1146.